Desalination and Water Treatment
www.deswater.com

doi: 10.5004/dwt.2019.23515

143 (2019) 352–365
March

Mechanism of decolorization of acid fuchsin by means of fixed iron ion and graphite electrode

Yunhai Wu[a,*], Ningning Liu[a], Zhu Ming[b]

[a]*Key Laboratory of Integrated Regulation and Resources Development of Shallow Lakes, Ministry of Education, Hohai University, Xikang Road #1, Nanjing, 210098, China, Tel./Fax: +86 25 83786697; emails: liuningningjy@163.com (Y. Wu), 18260057373@163.com (N. Liu)*
[b]*College of Environment, Hohai University, Xikang Road #1, Nanjing, 210098, China, Tel. +86 25 83786697; email: mingzhu0318@163.com*

Received 6 June 2018; Accepted 21 November 2018

ABSTRACT

Fe fixed with sodium alginate gel beads (Fe^{3+}-SA) was successfully synthesized. The application of the electro-Fenton (EF) technique using Fe^{3+}-SA for the degradation of acid fuchsin (AF) was investigated. The decolorization of AF by EF with Fe^{3+}-SA and homogeneous Fe^{3+} was studied, which confirmed that the EF with Fe^{3+}-SA could attain higher color removal rate (98.2%). Redox of Fe^{3+}-SA and homogeneous Fe^{3+} were also examined by cyclic voltammetry. Influencing factors on AF decolorization including pH, current density, initial AF concentration, Fe^{3+}-SA dosage, Cl^- concentration, were investigated by conducting batch experiments. The results showed that AF could be decolorized effectively in a wide pH range of 3–11. pH, applied current density, initial AF concentration, H_2O_2/Fe^{3+}-SA ratio, and the addition of Cl^- affected AF decolorization. The pseudo-first-order kinetic model can accurately describe the AF decolorization process. In addition, 100 mg/L AF was treated by EF with Fe^{3+}-SA for 4 h to evaluate total organic carbon (TOC) removal, mineralization current efficiency, and specific energy consumption. The properties of Fe^{3+}-SA, and Fe^{3+}-SA after EF reaction (Fe^{3+}-SA/EF) were characterized by scanning electron microscopy, Fourier-transform infrared spectroscopy, and X-ray photo-electron spectrometry. The iron content in AF solution before and after EF was measured by inductively coupled plasma atomic emission spectroscopy. Ion chromatography analyzed the change in inorganic salt during EF and ultraviolet–visible spectroscopy studied the decolorizing mechanism.

Keywords: Electro-Fenton; Acid fuchsin; Fe sodium alginate gel beads; Decolorization

1. Introduction

Many industries currently discharge into the environment a high percentage of wastewater containing dyes such as acid fuchsin (AF), and rhodamine B (RhB) [1,2]. The complex aromatic structures and xenobiotic properties of dyes hinder their degradation [3]. As a representative triphenylmethane dye, AF is often used as verification of free chlorine, colorant for connective tissue and pH indicator; it also has a highly-conjugated molecular system. However, its structure includes the benzene ring, which exerts a strong inhibitory effect on living things, impeding its biodegrade into small inorganic molecules.

Advanced oxidation processes (AOPs) have attracted considerable interest as potential methods for the efficient removal of wastewater [4–6]. AOPs are used in the production of a high-activity oxidant, principally hydroxyl radical (•OH), as their main oxidizing agent [7]. Among the AOPs, Fenton reagent (mixture of H_2O_2 and Fe^{2+}) has been widely used [8]. However, H_2O_2 is highly unstable; therefore, the application of the Fenton method is limited by the high cost of transportation and storage of H_2O_2 [9]. The Fenton method

* Corresponding author.

also requires the continuous addition of an iron catalyst because of the formation of iron sludge [10]. Compared with the Fenton method, electro-Fenton (EF) can produce mostly H_2O_2 in situ of cathode because of the use of an adequate electrode material. The reaction between H_2O_2 and Fe^{2+} added externally generates many •OH [11,12]. Thus, the EF method is more effective and easier to implement than the regular Fenton process [13–15]. The EF is a promising technology with relatively low energy consumption, highly organic mineralization degree, and effectively combines electrochemistry with the Fenton method [16]. The EF process operates depending on the in situ electro-generation of Fenton's reagent, which is the source of Fenton's reaction to generate hydroxyl radicals. A small amount of Fe^{2+} acts as catalyst, increasing the oxidizing ability of H_2O_2, forming Fe^{3+} and •OH [17]. One of the advantages of the EF process is the catalysis of Fenton's reaction by electrochemical regeneration of Fe^{2+} [18,19]. The entire process involves no secondary pollutants because Fe^{2+} and Fe^{3+} form a circulating system. The initial Fe^{2+} is also obtained from externally added Fe^{3+} [20]. EF has attracted significant attention for the efficient decolorization of dyes [21,22].

Despite its strong oxidation, traditional EF has several typical disadvantages. For instance, it needs to ensure acidic condition which can prevent soluble iron from precipitating. Recent studies have confirmed that mineral iron oxides, such as magnetite (Fe_3O_4) and wustite (FeO), can effectively degrade organic contaminants during EF at pH 3 [23]. Zero-valent iron at pH 2–4 can also be used as a catalyst for EF [24]. To overcome the limitation of pH and enlarge the scope of applications, the utilization of heterogeneous catalysts during EF reactions has drawn considerable attention. In previous studies [25–27], some heterogeneous catalysts can facilitate the removal efficiency of contaminants over a wide range of reaction pH, and diminish metal leaching during catalyst recycling. Fe^{3+}-SA has been used as source of iron in different environmental applications [28–30]. Fe^{3+} ions are coordinated with oxygen atoms which are in the carboxyl groups from the glucose chains of alginates, to form Fe^{3+}-SA. Iron binding on alginate beads decreases the negative effect of pH during EF process. Thus, EF can be used in a wide pH range of 2–8. In addition, the use of Fe^{3+}-SA allows the attainment of continuous operation.

This study aims to further explore the heterogeneous EF treatment using Fe^{3+}-SA. The comparison of the EF process operation with Fe^{3+}-SA and homogeneous Fe^{3+} was determined; cyclic voltammetry (CV) was used to examine the redox of Fe^{3+}-SA and homogeneous Fe^{3+}. The effects of the pH, current density, initial AF concentration, H_2O_2/Fe^{3+}-SA ratio, and Cl^- concentration on AF decolorization during EF using Fe^{3+}-SA were also evaluated. Meanwhile, the oxidation kinetics of the process was discussed. To further explore the oxidation capacity, mineralization rate, mineralization current efficiency and specific energy consumption, 100 mg/L AF solutions were examined at 20 mA/cm^2 current intensity, pH 3, and a H_2O_2/Fe^{3+}-SA ratio of 0.4. The TOC removal, mineralization current efficiency, and specific energy consumption were examined using 100 mg/L AF for 4 h. Moreover, the physicochemical characteristics of Fe^{3+}-SA and Fe^{3+}-SA/EF were examined with scanning electron microscopy (SEM), Fourier-transform infrared (FTIR) spectroscopy, and X-ray photo-electron spectrometry (XPS). The iron content in AF solution before and after EF treatment (AF/EF) was measured by inductively coupled plasma atomic emission spectrophotometer (ICP-AES). The degrading process was studied by ion chromatography (IC) and ultraviolet–visible spectroscopy (UV-Vis).

2. Materials and methods

2.1. Reagents

AF, sodium alginate (SA), and graphite electrodes provided by Sinopharm Chemical Reagent Co., Ltd. (China) were used during EF treatment. The AF characteristics and structure are described in Fig. S1. Sodium hydroxide, concentrated sulfuric acid (98%), anhydrous sodium sulfate, barium chloride, and ferric sulfate were purchased from Nanjing Ruitai Chemical Reagent Co. Ltd. (China). All chemicals were of analytical grade and used as received without further treatment and purification. Deionized water was used in all experiments.

2.2. Fe^{3+}-SA

Spherical alginate beads were formed by dropping 2.0% (w/v) SA (chemically pure) into 0.15 M Ba^{2+} ($BaCl_2{\cdot}2H_2O$), 0.05 M Fe^{3+} ($Fe_2(SO_4)_3$) solution [31]. The alginate beads presented brown particles after having been cured at room temperature for 2 h in the gelling solution. They were washed repeatedly with deionized water and finally stored in distilled water at 4°C for use in AF degradation.

2.3. Electrochemical reactor set up

EF experimental set-up is shown in Fig. 1. Batch EF experiments were conducted in a glass cylindrical reactor with a working volume of 0.25 L. The supporting electrolyte used was 0.05 M Na_2SO_4. During this process, H_2O_2 was generated by oxygen reduction on the graphite cathode. Bubbling compressed air near the cathode for 10 min before electrolysis at about 1 L/min ensured continuous saturation of air at atmospheric pressure [32,33]. The selected electrodes consisted of two graphite sheets which were connected to a power supply (HP model 3662; Agilent Technologies

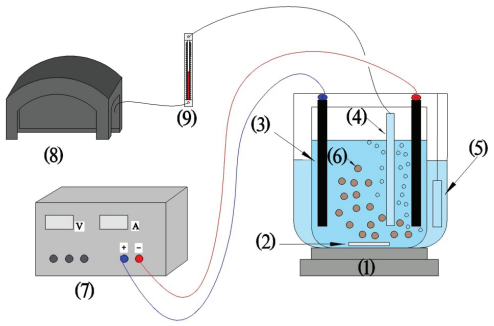

Fig. 1. EF experimental set-up: (1) magnetic stirring apparatus, (2) rotor, (3) graphite electrode, (4) temperature detector, (5) aeration device, (6) Fe^{3+}-SA, (7) power supply, (8) air pump, and (9) flow meter.

Spain, S.L.). Current density was measured using a multimeter (Fluke 175, America). The electrode sheets (surface area 15 cm^2) were placed opposite to each other at 1 cm above the bottom of the reactor and with an electrode gap of 6 cm [34]. A magnetic mixer with an automatic temperature control system (S25-2, Shanghai Sile Instrument Co., Ltd.) was used to control the temperature of the reaction solution at 25°C.

2.4. Electro-Fenton process

2.4.1. Comparison of Fe^{3+}-SA and homogeneous Fe^{3+} in EF

Fe^{3+}-SA at 467 mg and homogeneous Fe^{3+} (0.2 mM) were, respectively, applied to dispose 100 mg/L AF at pH 3 by applying 20 mA/cm^2 for 2 h [35]. The effect of Fe^{3+}-SA adsorption property on AF decolorization was also considered. Meanwhile, the electrochemical performances of Fe^{3+}-SA and homogeneous Fe^{3+} were investigated by CV under a three-electrode cell configuration at room temperature. A graphite electrode and a platinum wire served as the working electrode and the counter electrode, respectively. Meanwhile, the Ag/AgCl electrode was used as the reference electrode. A Na_2SO_4 solution at 0.05 M concentration and pH of 3 was used as the electrolyte and 467 mg Fe^{3+}-SA was added into the electrolyte. The electrolyte had to be deoxygenated with pure nitrogen for 30 min prior to the experiments.

2.4.2. Influence of experimental variables on EF

To obtain the best reaction conditions and study the reaction mechanism, the effects of pH, current density, initial AF solution concentration, H_2O_2/Fe^{3+}-SA ratio, and Cl^- concentration were discussed. Four concentrations of AF solutions, containing 100, 200, 300, and 400 mg/L were prepared. They were degraded comparatively by applying constant current densities of 5, 10, 15, 20, and 25 mA/cm^2 with H_2O_2/Fe^{3+}-SA ratios of 0.1, 0.2, 0.4, and 0.8 at initial pH of 3, 5, 7, 9, and 11 for 2 h. To measure the distraction of Cl^- when preparing Fe^{3+}-SA, the effect of Cl^- was also evaluated. Different Cl^- concentrations were added into the EF process with 100 mg/L AF and a H_2O_2/Fe^{3+}-SA ratio of 0.4 at pH 3, applying 20 mA/cm^2. The Cl^- concentrations were 0, 0.001, 0.01, and 0.1 M. The precise conditions for each test are listed in Table S1. In these experiments, pH was adjusted using 0.1 M NaOH or 0.1 M H_2SO_4. AF was stirred magnetically to avoid concentration gradients in the EF. In the experiments, samples were taken out from the EF reactor at regular intervals to be analyzed. Electric parameters were recorded. All samples were withdrawn from electrolyzed solutions centrifuged at 10,000 rpm for 5 min, and the supernatant was extracted for analysis.

2.4.3. Mineralization during EF reaction

Under the optimal conditions based on the aforementioned reaction, TOC of AF was measured. Thus TOC removal, mineralization current efficiency, and the specific energy consumption were calculated.

2.5. Characterization of samples in EF process

The CV measurement of the electrodes was conducted using an electrochemical workstation (CHI660D, Chenhua Instrument, China) between –2.0 and 1.0 V at a scan rate of 100 mV/s. The Fe^{3+}-SA samples before and after EF (Fe^{3+}-SA/EF) were ground into powder and then dried in an oven at 60°C for 40 min. The morphologies of Fe^{3+}-SA and Fe^{3+}-SA/EF samples were observed by SEM (S4800, Hitachi Ltd., Japan). The FTIR (Bruker Corporation, Germany) spectra of Fe^{3+}-SA and Fe^{3+}-SA/EF were recorded, and the spectra were in the 400–4,000 cm^{-1} range. XPS (PHI/5000 Versa Probe, ULVCA-PHI Corporation, USA) measurements of Fe^{3+}-SA and Fe^{3+}-SA/EF were performed with a monochromatic Mg-Kα source and a charge neutralizer. The iron content in the AF solution before and after EF was determined by ICP-AES (ICAP 6300, Thermo Scientific, USA). IC (ICS-1000, Sigma-Aldrich, USA) and UV–Vis (UV-1201, Ruili Analytical Instrument Corporation Ltd., China) were used to analyze the changes of inorganic salt and reaction mechanism during EF process.

2.6. Analytical methods

2.6.1. AF decolorization rate

The concentrations of AF were measured by a UV-spectrophotometer at a wavelength of 409 nm using the standard curve method. The standard AF concentration corresponded to absorbance, as shown in Table S2. The AF standard curve is presented in Fig. S2. The decolorization rate was calculated from Eq. (1) as follows:

$$D = \frac{(C_0 - C_t)}{C_0} \times 100\% \tag{1}$$

where D is the decolorization rate (%); C_0 and C_t are the initial concentration and concentration at time t, respectively.

The energy consumption per unit color removed for each decolorization trial [36] was then obtained using Eq. (2) as follows:

$$EC_{AF} = \frac{E_{cell} \times I \times t}{V \times \Delta(AF)_{exp}} \tag{2}$$

where EC_{AF} is the energy consumption per unit AF color removed (KWh/mol_{AF}), E_{cell} is the average cell voltage (V), I is the average applied current (A), t is time (h), and V is volume of AF (L), $\Delta(AF)_{exp}$ is the concentration variation of AF (mol/L).

A kinetic model was used to explain the effects of reaction conditions. Decolorization rate constant [37] was determined using a powder-law expression (Eq. (3)):

$$\frac{-d(C)}{d_t} = k \times (C)^n \tag{3}$$

where k represents the rate constant (min^{-1}), C is the AF concentration (mg/L), and n is the reaction order.

2.6.2. TOC analysis

The production of short-chain carboxylic acids was confirmed by the ion-exclusion chromatography analysis.

Mineralization of the AF solutions was verified from the decay of TOC. The percentage of TOC decay was determined using Eq. (4) as follows:

$$\mathrm{TOC}_{\mathrm{removal}} = \frac{\left(\mathrm{TOC}_0 - \mathrm{TOC}_t\right)}{\mathrm{TOC}_0} \times 100\% \tag{4}$$

where TOC_t and TOC_0 are the experimental TOC values at time t and the initial time, respectively.

According to these data, the mineralization current efficiency (MCE) for each treated solution [38] at the current I (A) and a given electrolysis time t (h) was estimated using Eq. (5) as follows:

$$\mathrm{MCE} = \frac{n \times F \times V_s \times \Delta\left(\mathrm{TOC}\right)_{\mathrm{exp}}}{4.32 \times 10^7 \times m \times I \times t} \times 100\% \tag{5}$$

where F is the Faraday constant (96,487 C/mol), V_s is the solution volume (L), $\Delta(TOC)_{\mathrm{exp}}$ is the experimental TOC decay (mg/L), and 4.32×10^7 is a conversion factor to homogenize units (3,600 s/h × 12,000 C/mol), and m is the number of carbon atoms of AF. The number of electrons n consumed per AF molecule was set to 90 so that AF was completely mineralized to CO_2, sulfate, and ammonium during mineralization, in accordance with Eq. (6) as follows:

$$\begin{aligned} &\mathrm{C_{20}H_{17}N_3Na_2O_9S_3} + 43\mathrm{H_2O} \rightarrow 20\mathrm{CO_2} + 3\mathrm{NH_4^+} \\ &\quad + 3\mathrm{SO_4^{2-}} + 2\mathrm{Na^+} + 91\mathrm{H^+} + 90\mathrm{e^-} \end{aligned} \tag{6}$$

Energy consumption per unit TOC mass destroyed ($\mathrm{EC_{TOC}}$) for each degradation trial was then obtained using Eq. (7) as follows:

$$\mathrm{EC_{TOC}} = \frac{E_{\mathrm{cell}} \times I \times t}{V_s \times \Delta\left(\mathrm{TOC}\right)_{\mathrm{exp}}} \tag{7}$$

where $\mathrm{EC_{TOC}}$ is energy consumption per unit TOC mass destroyed ($\mathrm{KWh/mg_{TOC}}$), E_{cell} is the average voltage of the cell (V).

2.6.3. Fe ion analysis

The Fe content in Fe^{3+}-SA was measured by ICP-AES. The powder was dissolved in 1 M HNO_3. The prepared sample was of high purity, corresponding to 3,578 mg/kg in mass of Fe^{3+}-SA.

2.6.4. H_2O_2 analysis

The concentration of accumulated H_2O_2 was determined by potassium permanganate titration under different current intensities [39]. The reaction principle is expressed as follows:

$$\begin{aligned} &2\mathrm{KMnO_4} + 3\mathrm{H_2SO_4} + 5\mathrm{H_2O_2} \rightarrow \\ &\quad \mathrm{K_2SO_4} + 2\mathrm{MnSO_4} + 5\mathrm{O_2} + 8\mathrm{H_2O} \end{aligned} \tag{8}$$

The 5 mL sample was transferred into an Erlenmeyer flask with a pipette, followed by 20 mL deionized water and 10 mL 20% H_2SO_4. Proven potassium permanganate was dropped into the sample and shaken until the solution became light red. All data used were the average of thrice test results.

$$C_{\mathrm{H_2O_2}} = \frac{\left(5 \times C_{\mathrm{K_2MnO_4}} \times V_{\mathrm{KMnO_4}}\right)}{2 \times V_{\mathrm{H_2O_2}}} \tag{9}$$

3. Results and discussion

3.1. Fe^{3+}-SA

Fe^{3+}-SA exhibited a spherical particle with an average diameter of 3.5 mm. The Fe^{3+}-SA was determined to include a Fe concentration of 3,584 mg/kg. Several polymer network gel beads could be applied in the removal of inorganic and organic contaminants from wastewater [40–43]. To eliminate the effect of adsorption, adsorption on AF by Fe^{3+}-SA was conducted at 100 mg/L AF solution for 2 h. The result indicated that AF adsorption was lower than 3% with the addition of 80 mg (maximum in the reaction) Fe^{3+}-SA. Therefore, the effect of adsorption during EF could be disregarded for 2 h.

3.2. Comparison of Fe3+-SA and homogeneous Fe3+ in EF

467 mg Fe^{3+}-SA and homogeneous Fe^{3+} (0.2 mM) were, respectively, used in EF process to treat 100 mg/L AF by applying 20 mA/cm^2 current density at pH 3 for 2 h. Homogeneous Fe^{3+} was provided by $Fe_2(SO_4)_3$. The change in AF decolorization rate is shown in Fig. 2(a). The AF decolorization rate by EF using Fe^{3+}-SA was higher than that using homogeneous Fe^{3+}, which indicated that the EF using Fe^{3+}-SA improved the AF decolorization rate to a certain degree. Meanwhile, Fig. 2(b) presents the CV curves conducted in 100 mg/L AF containing 0.05 M Na_2SO_4 at pH 3. The reduction in O_2 on the surface of the graphite electrode was vital for the electro-generation of H_2O_2. CV curves illustrated the effect of Fe^{3+}-SA and homogeneous Fe^{3+} on the reduction/oxidation of Fe ions and the over potential of O_2 reduction on the surface of the graphite electrode. Reduction peaks in homogeneous Fe^{3+} at –0.3 and 0.2 V were observed, which were identified as reduction peaks of O_2 or Fe^{3+}. However, the reduction peaks shifted to –0.46 and 0.06 V with a markedly increased current for Fe^{3+}-SA, which indicated that Fe^{3+}-SA reduced the over-potential of O_2 and Fe^{3+} reduction on the surface of the cathode material. Thus, a reduction reaction was easier than before [44]. In addition, a redox peak belonging to Fe^{2+} could be observed within this potential range. The alginate polymer was not electrochemically active in the applied potential range [45]. Therefore, the redox process was related to the reduction/oxidation of Fe ions which used as the cross-linkers in the Fe^{3+}-SA.

3.3. Influencing factors

3.3.1. pH

Electrolysis was conducted performed at initial pH levels of 3, 5, 7, 9, and 11 in the 100 mg/L AF containing the 0.4

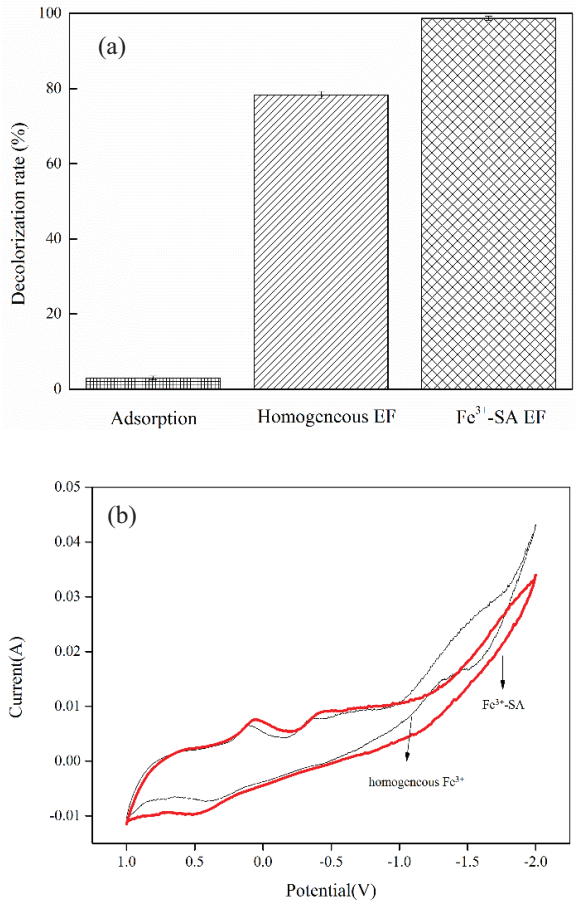

Fig. 2. Decolorization on AF by EF using Fe^{3+}-SA and homogeneous Fe^{3+} with H_2O_2/Fe^{3+}-SA ratio 0.4, 0.05 M Na_2SO_4, 100 mg/L AF, 20 mA/cm^2 current density and pH 3 (a); comparison of CV of Fe^{3+}-SA and homogeneous Fe^{3+}; conditions: pH 3, 0.05 M Na_2SO_4, air flow rate 1.0 L min^{-1} (b).

H_2O_2/Fe^{3+}-SA ratios by applying 20 mA/cm^2 current density. The changes in AF concentration under different pH levels are illustrated in Fig. 3. The acid condition benefited AF decolorization during the EF process. But under extreme acid conditions, the concentration of H^+ was considerably high, and H_2O_2 reacted with many H^+ to form $H_3O_2^+$ (Eq. (12)). Increased $H_3O_2^+$ enhanced the stability of Fe^{3+} and decreased the activity of Fe^{3+} [46,47], and the scavenging effect of the •OH by H^+ became severe (Eq. (13)). Under alkaline conditions, the cross-linking of Fe^{3+}-SA could be destroyed slightly, and Fe^{3+} was leached, leading to the generation of iron hydroxides. Meanwhile, H_2O_2 was unstable in alkaline solutions and was quickly decomposed into oxygen and water (Eq. (10)), which led to the loss of its oxidizing ability. A previous study reported that homogeneous EF treatment exhibited a slight reduction in decolorization rates under alkaline conditions or at neutral pH [27]. Fig. 3 shows that all AF decolorization rates are higher than 80% in the final stage, and the pH remains almost unchanged in an alkaline environment. This performance confirmed that Fe^{3+}-SA could be applicable in a larger scale of pH. As shown in Fig. 3, the concentration of AF declined exponentially which was in accordance with pseudo-first-order kinetics. The graph exhibited a high linear

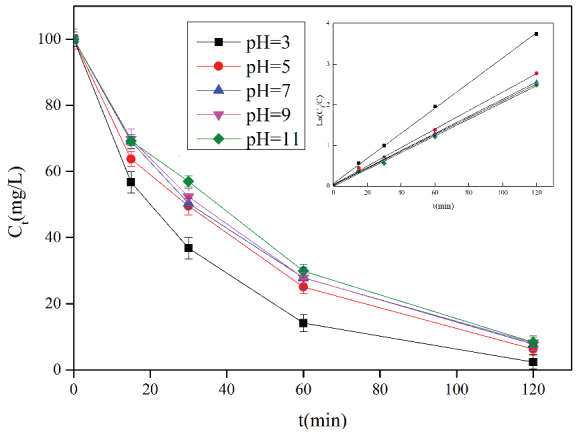

Fig. 3. Effect of pH on decolorization of AF by EF with 0.4 H_2O_2/Fe^{3+}-SA ratio, 0.05 M Na_2SO_4, 100 mg/L AF, and 20 mA/cm^2 current density.

correlation. In summary, pH of 3 was most contributed to the effective degradation of AF.

$$H_2O_2 \rightarrow H_2O + O_2 \quad (10)$$

$$H_2O_2 + H^+ \rightarrow H_3O_2^+ \quad (11)$$

$$\bullet OH + H^+ + e^- \rightarrow H_2O \quad (12)$$

3.3.2. Applied current density

To explore the effects of applied current on AF decolorization, different current densities ranging from 5 to 25 mA/cm^2 were studied. The changes in AF concentration under different current densities are presented in Fig. 4(a), which illustrates an increase in AF decolorization when the current density increased from 5 to 25 mA/cm^2. Meanwhile, the oxidizing power is related to the increased production of H_2O_2, which led to the generation of •OH [48], as shown in Eqs. (13) and (14). High current density produced other oxides, such as $S_2O_8^{2-}$ and O_3, which could also degrade AF. An excessively high current density (25 mA/cm^2) may induce anodic oxygen evolution reaction and cathode hydrogen evolution reaction, inhibiting the direct oxidation of AF.

$$O_2(g) + 2H^+ + 2e^- \rightarrow H_2O_2 \quad (13)$$

$$Fe^{2+} + H_2O_2 \rightarrow Fe^{3+} + \bullet OH + OH^- \quad (14)$$

Fig. 4(b) proved that the production of H_2O_2 related to current intensity. AF decolorization did not grow linearly with an increase in reaction time because H_2O_2 concentration reached its steady-state after about 120 min. Meanwhile, this increase in applied current exerted no significant effect on color removal (Fig. 4(a)). The reason could be that during electrolysis, AF was quickly degraded by hydroxyl radicals which were formed by the Fe^{2+} that transferred from the Fe^{3+}

of Fe^{3+}-SA (Eq. (15)), allowing the gradual formation of intermediates that were difficult to destroy, as complexes of Fe^{3+} and carboxylic acid [49].

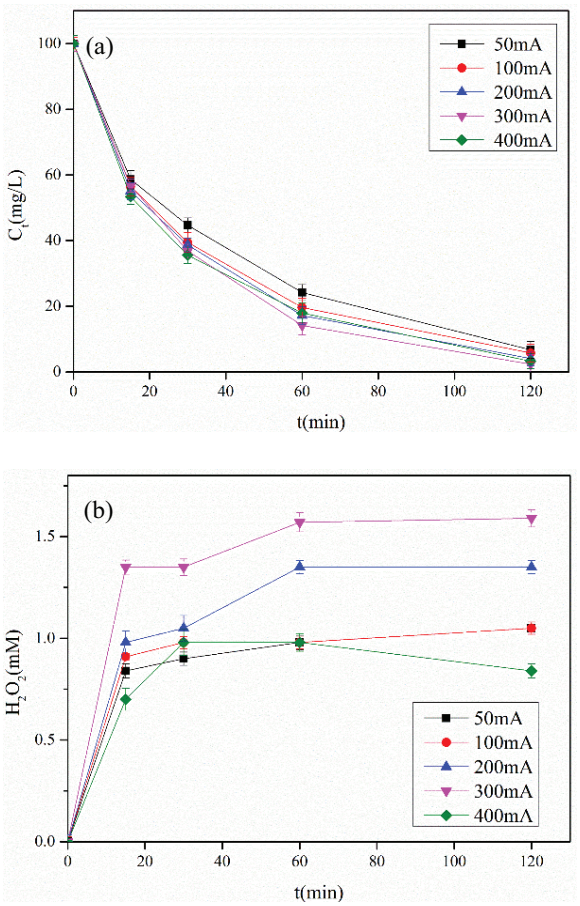

Fig. 4. Effect of applied current intensity on decolorization of AF by EF with 0.4 H_2O_2/Fe^{3+}-SA ratio, 0.05 M Na_2SO_4, 100 mg/L AF, and pH 3 (a); effect of applied current intensity on production of H_2O_2 with 0.4 H_2O_2/Fe^{3+}-SA ratio, 0.05 M Na_2SO_4, 100 mg/L AF, and pH 3 (b).

$$Fe^{3+} + e \rightarrow Fe^{2+} \quad (15)$$

Moreover, the production of H_2O_2 decreased at 400 mA (Fig. 4(b)), and black powder particles were found in the AF solution after EF. The increase in applied current might have promoted the parasitic reactions, such as hydrogen evolution at the cathode.

3.3.3. Initial AF concentration

Fig. 5(a) presents the decolorization performance of EF process at various AF concentrations. With an increase in AF concentrations, the decolorization rate slightly decreased. This behavior was attributable to the physicochemical properties of contaminants and steric effects. More hydroxyl radicals were required for the degradation of AF and reaction of intermediates at higher AF concentrations. Meanwhile, the solution pH rapidly decreased because more carboxylic acids were produced at higher AF concentrations.

3.3.4. Fe^{3+}-SA dosage

The influence of Fe^{3+}-SA dosage on AF decolorization was evaluated by applying 300 mA at pH 3 during EF to a solution of 100 mg/L AF (Fig. 5(b)). These conditions had small variations. The result showed that few ferrous ions would expend most hydroxyl radicals, and that Fe ion cycle continued because only few catalysts were precipitated. Consequently, no improvement of AF decolorization rate occurred with an enhancement in Fe^{3+}-SA dosage.

3.3.5. Addition of Cl^-

Fig. 6 shows that the introduction of Cl^- was considered as interference on AF decolorization during EF. When Cl^- was 0, 0.001, and 0.01 M, the trend of decolorization rate was nearly uniform. This finding proved that Cl^- only slightly influenced AF decolorization when HCl was used to adjust the pH [50]. However, the AF concentration markedly decreased at Cl^- equal to 0.1 M, and the color removal rate reached 98.8% after 15 min. The reason could be that Cl^- was discharged at the

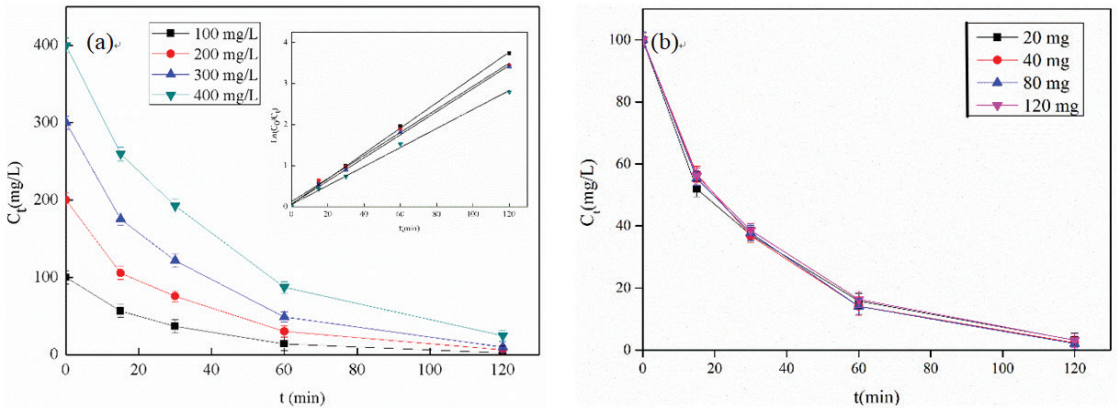

Fig. 5. Effect of the AF concentration on decolorization of AF by EF with 0.4 H_2O_2/Fe^{3+}-SA ratio, 0.05 M Na_2SO_4, 20 mA/cm^2 current density, and pH 3 (a); effect of the Fe^{3+}-SA dosage on decolorization of AF by EF with 100 mg/L AF, 0.05 M Na_2SO_4, 20 mA/cm^2 current density, and pH 3 (b).

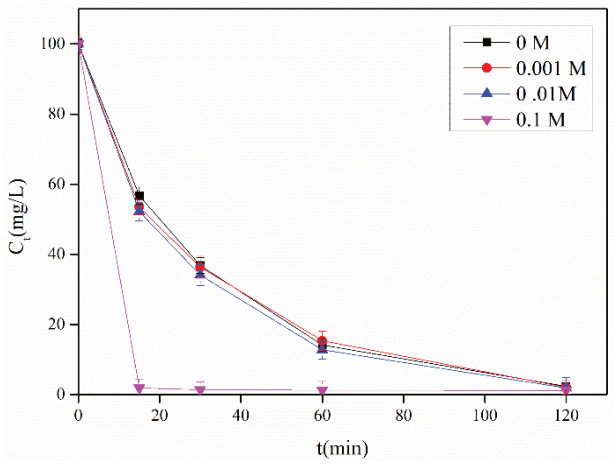

Fig. 6. Effect of Cl^- on decolorization of AF by EF with 0.4 H_2O_2/Fe^{3+}-SA ratio, 0.05 M Na_2SO_4, 100 mg/L AF, 20 mA/cm² current density, and pH 3.

anode to generate Cl_2, which was immediately dissolved in the solution and, chemically converted to ClO^- [2]. ClO^- could effectively oxidize AF. To obtain better search results, pH of 3 was selected as an appropriate condition.

3.4. Kinetics study

Kinetic studies were conducted to determine the kinetic behavior of AF decolorization process. Fig. 7(a) shows the change in AF concentration at 300 mA for 4 h. As shown in Fig. 7(b), the rate constant values (0.028) and the statistical correlation parameters (R^2 = 0.967) obtained from the model fitting reflected that AF decolorization process conformed to the pseudo-first-order kinetics. When the electrocatalytic reaction occurred, the initial concentration of H_2O_2 was zero and then accumulated. Eq. (16) describes the relationship between the production of •OH and the concentration of Fe^{2+} and H_2O_2. The high concentration of H_2O_2 led to the rapid generation of •OH and subsequently resulted in a high AF decolorization rate.

$$\bullet OH = \lambda \times \left(d\left[\bullet OH\right]/dt\right)_g = \lambda \times k\left[Fe^{2+}\right] \times \left[H_2O_2\right] \quad (16)$$

where k is the apparent rate constant, λ is the rate constant, •OH represents the production of •OH, $[Fe^{2+}]$ and $[H_2O_2]$ are the concentration of Fe^{2+} and H_2O_2 (mg/L), respectively. A comparison of the maximum AF decolorization rate by different treatment methods is shown in Table S3 [51,52].

3.5. Energy consumption during the EF

To establish the viability of Fe^{3+}-SA in AF decolorization by EF, the energy consumption per concentration removed (EC_{AF}) was assessed. Fig. 8 shows the energy cost of AF decolorization calculated from Eq. (2). For low AF decolorization rate, the specific energy consumption increased almost linearly, and became exponential for high AF decolorization rate. It can be explained that more refractory products and hardly oxidizable intermediates might

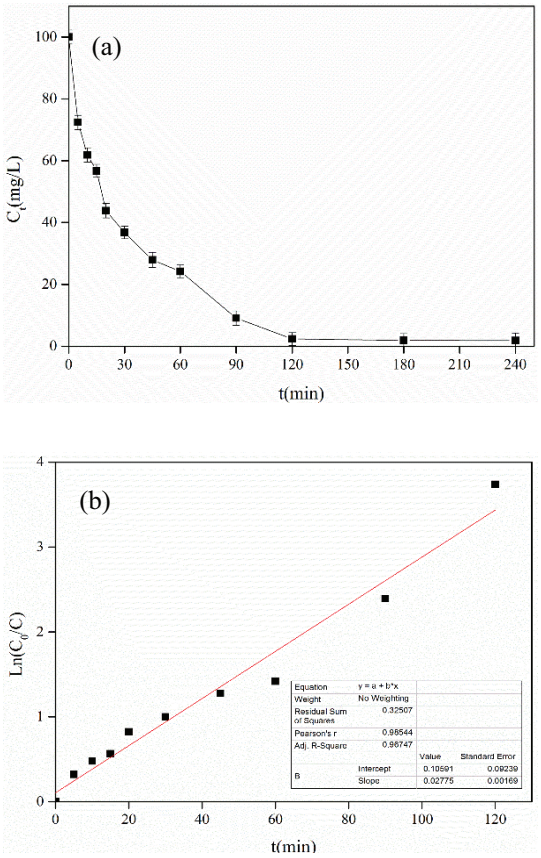

Fig. 7. Trend of concentration degradation of AF by EF with 0.4 H_2O_2/Fe^{3+}-SA ratio, 0.05 M Na_2SO_4, 100 mg/L AF, 20 mA/cm² current density and pH 3 (a); pseudo-first-order kinetics of AF by EF process with 0.4 H_2O_2/Fe^{3+}-SA ratio, 0.05 M Na_2SO_4, 100 mg/L AF, 20 mA/cm² current density and pH 3 (b).

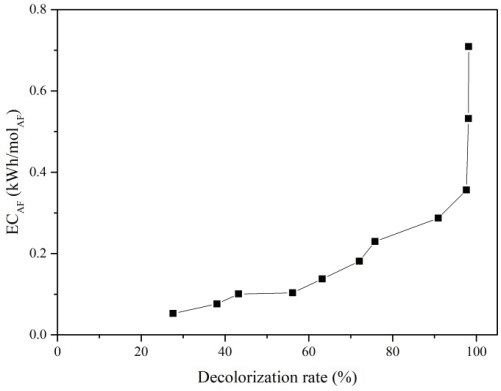

Fig. 8. Energy consumption per unit concentration with 0.4 H_2O_2/Fe^{3+}-SA ratio, 0.05 M Na_2SO_4, 100 mg/L AF, 20 mA/cm² current density and pH 3.

have been formed, such as short-chain carboxylic acids. Moreover, low organic content led to parasitic reaction. When the AF decolorization rate to 98.6%, the energy consumption reached 0.7 kWh/(mol_{AF}). It confirmed that low energy consumption was achieved during the process.

3.6. Mineralization of AF

IC was used to quantify inorganic ions formed during the electro-Fenton treatment process of AF. The chromatograms revealed the formations of three different ions: ammonium, nitrate, and sulfate. As shown in Fig. S3, ammonium and sulfate were the most rapidly released ions within 120 min. The release of sulfate was almost stoichiometric (0.50 instead of 0.51 mM). Moreover, the concentration of nitrate was considerably low during electrolysis. Total concentration of NH_4^+ and NO_3^- (0.44 mM) was 86.2% of the initial amount of nitrogen. The mineralization of AF was detected in 100 mg/L AF with the 0.4 H_2O_2/Fe^{3+}-SA ratio, by 300 mA current intensity at pH 3; 44.0% TOC removal was achieved after 2 h of treatment because of the formation and accumulation of some oxidation by-products [44]. Notably, 84.8% TOC removal was achieved after 4 h. Total mineralization requires more time, perhaps because the formation of Fe(III)–carboxylate complexes, which were hardly oxidized by •OH [53].

The MCE was calculated in accordance with Eq. (5). The decrease in MCE could be attributable to several reasons, including the mass formation of persistent intermediates such as short-chain carboxylic acids, mass transport limitation caused by the loss of organic matter concentration, and the acceleration of the aforementioned waste reactions [54].

The energy consumption per unit TOC mass destroyed (EC_{TOC}) for each degradation trial was calculated from Eq. (7). Specific energy consumption increased linearly as the removal rate increased, becoming exponential for higher TOC removal rates. This occurrence could be attributable to the formation of more refractory products such as short-chain carboxylic acids, which were hardly oxidized intermediates, and the decrease in organic content in the solution which promoted parasitic reactions [55].

3.7. Characteristic of Fe^{3+}-SA and Fe^{3+}-SA/EF

3.7.1. Surface morphology of Fe^{3+}-SA and Fe^{3+}-SA/EF

The surface morphologies of the Fe^{3+}-SA and Fe^{3+}-SA/EF, which were obtained by SEM, are presented in Fig. S4. In Fig. S4(a), the surface of Fe^{3+}-SA is regularly undulating with a flocculent structure. Numerous changes in surface morphologies were observed after the EF process. Fig. S4(b) shows the transformation of a smooth surface into a rough surface. Fe^{3+}-SA/EF appeared with an irregularly porous structure.

3.7.2. FTIR spectra of Fe^{3+}-SA and Fe^{3+}-SA/EF

The FTIR spectra of Fe^{3+}-SA and Fe^{3+}-SA/EF are presented in Fig. S5. For both hydrogels, CH_2 vibrations appeared at 1,440 cm^{-1} [56]. The stretching of –C=O observed at 1,650 cm^{-1} contributed to the absorption vibrations of the carboxyl group of the alginate molecule [57,58]. The absorption bands at 640 and 2,860 cm^{-1} were assigned to Fe–O–H and C–H vibration, respectively [59]. Significant differences in FTIR spectra were observed between Fe^{3+}-SA and Fe^{3+}-SA/EF. The band in the spectrum at 1,200 and 2,300 cm^{-1} shifted slightly to 1,230 and 2,310 cm^{-1}, respectively. The change of bond strength between metal ions resulted in stretching vibration of the C–O bond. The change in oxygen of the carboxyl caused a change in vibration distance of C=N bond. These results confirmed that the reaction required a bit energy vibration. Notably, additional absorption bands appeared in the FTIR spectra of and Fe^{3+}-SA/EF at 1,180 and 2,400 cm^{-1}. The distinct 1,180 cm^{-1} band might correspond to O–H deformation and C–O stretching vibration interaction. This characteristic peak of Fe^{3+}-SA/EF at 2,400 cm^{-1} was observed and could be caused by the introduction of ammonium salts during the reaction.

3.7.3. XPS analyses of Fe^{3+}-SA and Fe^{3+}-SA/EF

XPS analyses were carried out to further investigate the bonding configuration of Fe in Fe^{3+}-SA during the EF reaction. Table S4 reveals that Fe^{3+}-SA is composed of C, O, Cl, Ba, and Fe. However, the Cl is not observed in Fe^{3+}-SA/EF (Fig. S6). The conclusion that could be drawn was that low Cl^- was participated in the reaction, which consisted with the consequence obtained in section 3.3.5. The percentage composition of Fe decreased slightly because leaching of a small amount of Fe occurred during EF. Fig. 9(a) shows that, for the Fe 2p spectrum, two photoelectron peaks center at 708.385 and 723.469 eV corresponding to the binding energies of Fe $2p_{3/2}$ and Fe $2p_{1/2}$, respectively. The peaks at 709.353 and 722.042 eV in Fig. 9(b) suggest the existence of Fe^{2+} [60]. The peak of Fe^{3+}-SA at 708.385 eV was narrower than that of Fe^{3+}-SA/EF at 709.353 eV. The intensity of the peaks decreased and an obvious shift occurred, suggesting that the valence state of Fe^{3+} changed during the EF process (Eq. (15)).

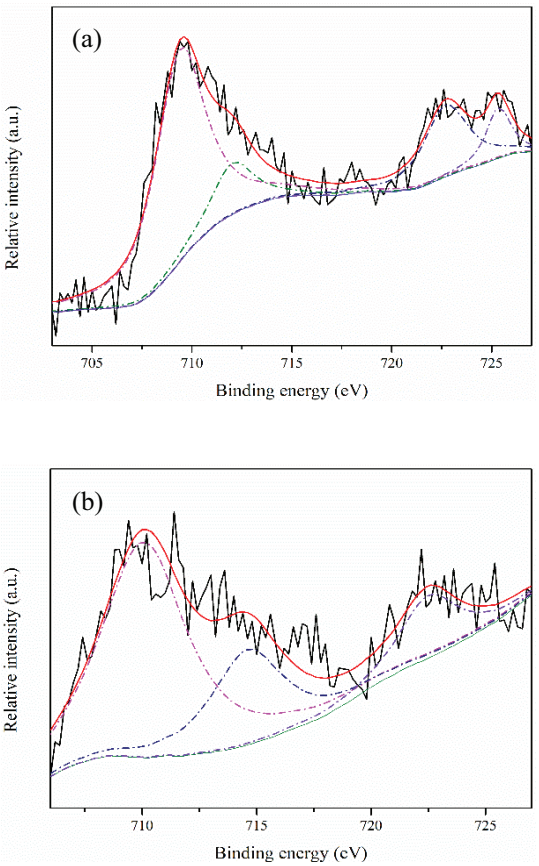

Fig. 9. XPS spectra of Fe region of Fe^{3+}-SA (a) and Fe^{3+}-SA/EF (b).

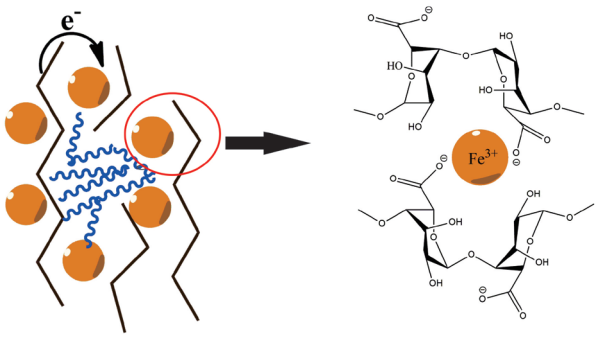

Fig. 10. Structure of Fe^{3+}-SA.

3.8. UV–visible absorption spectrum of AF

The UV–visible absorption spectrum of the AF solution at different reaction time is shown in Fig. S7. AF had two absorption peaks in the ultraviolet region at 208 and 283 nm, and absorption peaks in the visible region at 540 nm. The absorption peak in the visible region was corresponding to the AF chromophore absorption peak, which was mainly related to the three vinyl groups in the molecular structure of AF, whereas the absorption peak in the ultraviolet region was mainly related to the benzene ring, amino group, and sulfonic acid group in the AF structure [61]. As shown in Fig. S7, with an increase in EF reaction time, the three absorption peaks of AF in the entire UV-visible region were gradually decreased. After a 30 min EF reaction, the absorption peak of AF at 540 nm significantly decreased, indicating that the decolorization effect was significant. After a 120-min reaction, the absorption peak at 283 nm decreased significantly, but the removal rate of the absorption peak at 208 nm only slightly changed. During AF decolorization using EF, the vinyl was first destroyed rapidly. As the reaction proceeded, the benzene ring, amino group, and sulfonate group were gradually oxidized. No other absorption peaks appear, indicating that the intermediate products were gradually degraded.

3.9. Iron contents in AF and AF/EF

The iron contents in AF and AF/EF determined by ICP-AES analysis are listed in Table S5. Few Fe ions were found in AF/EF, suggesting that Fe^{3+} had hardly been leached. The structure of Fe^{3+}-SA is shown in Fig. 10. The "egg-box" structure was formed when alginate came in contact with Fe^{3+} [45]. The guluronate on the alginate chain lumped, causing the ions to cross join. Thus, alginate droplets immersed into ferrous aqueous solution could generate ionic cross-links between the carboxyl group on alginate chains and Fe [35]. A small number of Fe^{3+} ions overflowed during EF process could be explained that few ionic cross-links were destroyed. The reaction equation (Eq. (14)) could continue because of electrons passing in or out during the entire reaction. This result clearly shows that Fe^{3+} undergoes chemical reduction on the surface of Fe^{3+}-SA.

4. Conclusions

In this study, Fe^{3+}-SA was successfully developed for EF treatment. The results of this paper indicated that sodium alginate was an appropriate support for iron retention. The fixation of Fe into alginate beads induced the limitation of pH in the EF process. The use of Fe^{3+}-SA made EF can operate in a wide pH range of 3-11. The current intensity controlled the reaction rate because the production of H_2O_2 changed at different current intensities. The process obeyed pseudo-first-order kinetic model with the most fitting coefficient exceeding 0.985 and a removal efficiency of 98% under the following conditions: 100 mg/L AF, 0.4 H_2O_2/Fe^{3+}-SA ratio, 300 mA current intensity, and pH 3. Approximately 84.8% mineralization was achieved by applying Fe^{3+}-SA into the mineralization of AF solution. The characterization of Fe^{3+}-SA and Fe^{3+}-SA/EF showed that Fe was homogeneously distributed into the gel beads. Moreover, iron embedded in the sodium alginate could be protected from leaching during the reaction. The Fe^{3+}-SA exhibited stability, and Fe^{3+} was fixed in the alginate structure. Oxidative degradation of AF under the EF process using Fe^{3+}-SA in a continuous batch can be achieved.

Acknowledgment

This work was supported by a project funded by the Priority Academic Program Development of Jiangsu Higher Education Institutions.

References

[1] V.K. Gupta, R. Jain, S. Varshney, Removal of Reactofix golden yellow 3 RFN from aqueous solution using wheat husk--an agricultural waste, J. Hazard. Mater., 142 (2007) 443–448.
[2] Q. Husain, Peroxidase mediated decolorization and remediation of wastewater containing industrial dyes: a review, Rev. Environ. Sci. Bio-Technol., 9 (2010) 117–140.
[3] E. Rosales, M. Pazos, M.A. Sanromán, Comparative efficiencies of the decolourisation of leather dyes by enzymatic and electrochemical treatments, Desalination, 278 (2011) 312–317.
[4] Q. Ge, W. Peng, C. Wan, T.S. Chung, Polyelectrolyte-promoted forward osmosis-membrane distillation (FO-MD) hybrid process for dye wastewater treatment, Environ. Sci. Technol., 46 (2012) 6236–6243.
[5] Y. Juang, E. Nurhayati, C. Huang, J.R. Pan, S. Huang, A hybrid electrochemical advanced oxidation/microfiltration system using BDD/Ti anode for acid yellow 36 dye wastewater treatment, Sep. Purif. Technol., 120 (2013) 289–295.
[6] Y. Zhang, Y. Yanwen, J. Zhiqiang, Z. Quan, Steady performance of a zero valent iron packed anaerobic reactor for azo dye wastewater treatment under variable influent quality, J. Environ. Sci., 24 (2012) 720–727.
[7] E. Rosales, M. Pazos, M.A. Longo, M.A. Sanromán, Electro-Fenton decoloration of dyes in a continuous reactor: a promising technology in colored wastewater treatment, Chem. Eng. J., 155 (2009) 62–67.
[8] F. Emami, A.R. Tehrani-Bagha, K. Gharanjig, F.M. Menger, Kinetic study of the factors controlling Fenton-promoted destruction of a non-biodegradable dye, Desalination, 257 (2010) 124–128.
[9] A. Romero, A. Santos, T. Cordero, J. Rodríguez-Mirasol, J.M. Rosas, F. Vicente, Soil remediation by Fenton-like process: phenol removal and soil organic matter modification, Chem. Eng. J., 170 (2011) 36–43.
[10] A.B. dos Santos, F.J. Cervantes, J.B. van Lier, Review paper on current technologies for decolourisation of textile wastewaters: perspectives for anaerobic biotechnology, Bioresour. Technol., 98 (2007) 2369–2385.
[11] B. Balci, N. Oturan, R. Cherrier, M.A. Oturan, Degradation of atrazine in aqueous medium by electrocatalytically generated hydroxyl radicals. A kinetic and mechanistic study, Water Res., 43 (2009) 1924–1934.

[12] N. Oturan, M. Hamza, S. Ammar, R. Abdelhédi, M.A. Oturan, Oxidation/mineralization of 2-Nitrophenol in aqueous medium by electrochemical advanced oxidation processes using Pt/carbon-felt and BDD/carbon-felt cells, J. Electroanal. Chem., 661 (2011) 66–71.
[13] J.M. Friedrich, C. Ponce-De-León, G.W. Reade, F.C. Walsh, Reticulated vitreous carbon as an electrode material, J. Electroanal. Chem., 561 (2004) 203–217.
[14] E. Guinea, C. Arias, P.L. Cabot, J.A. Garrido, R.M. Rodríguez, F. Centellas, E. Brillas, Mineralization of salicylic acid in acidic aqueous medium by electrochemical advanced oxidation processes using platinum and boron-doped diamond as anode and cathodically generated hydrogen peroxide, Water Res., 42 (2008) 499–511.
[15] M.A. Oturan, R. Abdelhedi, N. Oturan, M. Asma, S. Ammar, Electrochemical degradation of anthraquinone dye Alizarin Red: role of the electrode material, Curr. Org. Chem., 16 (2012) 1978–1985.
[16] T.X.H. Le, M. Bechelany, S. Lacour, N. Oturan, M.A. Oturan, M. Cretin, High removal efficiency of dye pollutants by electron-Fenton process using a graphene based cathode, Carbon, 94 (2015) 1003–1011.
[17] M. Zhou, Q. Tan, Q. Wang, Y. Jiao, N. Oturan, M.A. Oturan, Degradation of organics in reverse osmosis concentrate by electro-Fenton process, J. Hazard. Mater., 215 (2012) 287–293.
[18] M. Panizza, M.A. Oturan, Degradation of Alizarin Red by electro-Fenton process using a graphite-felt cathode, Electrochim. Acta, 56 (2011) 7084–7087.
[19] E. Rosales, M. Pazos, M.A. Sanromán, Advances in the electro-Fenton process for remediation of recalcitrant organic compounds, Chem. Eng. Technol., 35 (2012) 609–617.
[20] Y. Fan, Z. Ai, L. Zhang, Design of an electro-Fenton system with a novel sandwich film cathode for wastewater treatment, J. Hazard. Mater., 176 (2010) 678–684.
[21] I. Sirés, E. Brillas, M.A. Oturan, M.A. Rodrigo, M. Panizza, Electrochemical advanced oxidation processes: today and tomorrow. A review, Environ. Sci. Pollut. Res., 21 (2014) 8336–8367.
[22] E. Brillas, C.A. Martínez-Huitle, Decontamination of wastewaters containing synthetic organic dyes by electrochemical methods. An updated review, Appl. Catal., B, 166–167 (2015) 603–643.
[23] E. Expósito, C.M. Sánchez-Sánchez, V. Montiel, Mineral iron oxides as iron source in electro-Fenton and photoelectro-Fenton mineralization processes, J. Electrochem. Soc., 154 (2007) E116–E122.
[24] M. Kallel, C. Belaid, T. Mechichi, M. Ksibi, B. Elleuch, Removal of organic load and phenolic compounds from olive mill wastewater by Fenton oxidation with zero-valent iron, Chem. Eng. J., 150 (2009) 391–395.
[25] E. Bocos, M. Pazos, M.A. Sanromán, Electro-Fenton decolourization of dyes in batch mode by the use of catalytic activity of iron loaded hydrogels, J. Chem. Technol. Biotechnol., 89 (2014) 1235–1242.
[26] L. Bounab, O. Iglesias, E. Gonzalez-Romero, M. Pazos, M.A. Sanroman, Effective heterogeneous electro-Fenton of m-cresol with iron loaded active carbon, RSC Adv., 5 (2015) 31049–31056.
[27] O. Iglesias, J. Gómez, M. Pazos, M.Á. Sanromán, Electro-Fenton oxidation of imidacloprid by Fe alginate gel beads, Appl. Catal., B, 144 (2014) 416–424.
[28] F.D.D. María Ángeles, D.C. Araceli González, F. Francisco Jesús, R. Manuel, P. Marta, S. María Ángeles, Bacterial-fungal interactions enhance power generation in microbial fuel cells and drive dye decolourisation by an ex situ and in situ electro-Fenton process, Bioresour. Technol., 148 (2013) 39–46.
[29] Y. Dong, W. Dong, Y. Cao, Z. Han, Z. Ding, Preparation and catalytic activity of Fe alginate gel beads for oxidative degradation of azo dyes under visible light irradiation, Catal. Today, 175 (2011) 346–355.
[30] O. Iglesias, F.D.D. Ma, M. Pazos, M.A. Sanromán, Using iron-loaded sepiolite obtained by adsorption as a catalyst in the electro-Fenton oxidation of Reactive Black 5, Environ. Sci. Pollut. Res., 20 (2013) 5983–5993.
[31] K. Hojeong, H.J. Hong, J. Juri, K. Seonghye, J.W. Yang, Degradation of trichloroethylene (TCE) by nanoscale zero-valent iron (nZVI) immobilized in alginate bead, J. Hazard. Mater., 176 (2010) 1038–1043.
[32] S.A. Messele, O.S.G.P. Soares, J.J.M. Órfão, C. Bengoa, F. Stüber, A. Fortuny, A. Fabregat, J. Font, Effect of activated carbon surface chemistry on the activity of ZVI/AC catalysts for Fenton-like oxidation of phenol, Catal. Today, 240 (2015) 73–79.
[33] M.A. Oturan, I. Sirés, N. Oturan, S. Pérocheau, J.L. Laborde, S. Trévin, Sonoelectro-Fenton process: a novel hybrid technique for the destruction of organic pollutants in water, J. Electroanal. Chem., 624 (2008) 329–332.
[34] O. Iglesias, M.A.F.D. Dios, E. Rosales, M. Pazos, M.A. Sanromán, Optimisation of decolourisation and degradation of Reactive Black 5 dye under electro-Fenton process using Fe alginate gel beads, Environ. Sci. Pollut. Res., 20 (2013) 2172–2183.
[35] E. Rosales, O. Iglesias, M. Pazos, M.A. Sanromán, Decolourisation of dyes under electro-Fenton process using Fe alginate gel beads, J. Hazard. Mater., 213–214 (2012) 369–377.
[36] E. Alfaya, O. Iglesias, M. Pazos, M. Sanroman, Environmental application of an industrial waste as catalyst for the electro-Fenton-like treatment of organic pollutants, RSC Adv., 5 (2015) 14416–14424.
[37] J. Virkutyte, E. Rokhina, V. Jegatheesan, V. Jegatheesan, L. Shu, H.H. Ngo, Optimisation of Electro-Fenton denitrification of a model wastewater using a response surface methodology, Bioresour. Technol., 101 (2010) 1440–1446.
[38] E.J. Ruiz, A. Hernández-Ramírez, J.M. Peralta-Hernández, C. Arias, E. Brillas, Application of solar photoelectro-Fenton technology to azo dyes mineralization: effect of current density, Fe^{2+} and dye concentrations, Chem. Eng. J., 171 (2011) 385–392.
[39] R.M. Sellers, Spectrophotometric determination of hydrogen peroxide using potassium titanium(IV) oxalate, Analyst, 105 (1980) 950–954.
[40] Y.S. Jeon, J. Lei, J.H. Kim, Dye adsorption characteristics of alginate/polyaspartate hydrogels, J. Ind. Eng. Chem., 14 (2008) 726–731.
[41] B. Kusuktham, Preparation of interpenetrating polymer network gel beads for dye absorption, J. Appl. Polym. Sci., 102 (2006) 1585–1591.
[42] G. Li, Y. Du, Y. Tao, H. Deng, X. Luo, J. Yang, Iron(II) cross-linked chitin-based gel beads: preparation, magnetic property and adsorption of methyl orange, Carbohydr. Polym., 82 (2010) 706–713.
[43] A. Santos, F.H.A. Silva, D.A. Maria, J.D. Ardisson, M.B. Franco, Synthesis and characterization of iron-PVA hydrogel microspheres and their use in the arsenic (V) removal from aqueous solution, Chem. Eng. J., 210 (2012) 432–443.
[44] M. Panizza, A. Dirany, I. Sirés, M. Haidar, N. Oturan, M.A. Oturan, Complete mineralization of the antibiotic amoxicillin by electro-Fenton with a BDD anode, J. Appl. Electrochem., 44 (2014) 1327–1335.
[45] Z. Jin, G. Güven, V. Bocharova, J. Halámek, I. Tokarev, S. Minko, A. Melman, D. Mandler, E. Katz, Electrochemically controlled drug-mimicking protein release from iron-alginate thin-films associated with an electrode, ACS Appl. Mater. Interfaces, 4 (2012) 466–475.
[46] M.M. Ghoneim, H.S. El-Desoky, N.M. Zidan, Electro-Fenton oxidation of Sunset Yellow FCF azo-dye in aqueous solutions, Desalination, 274 (2011) 22–30.
[47] J. Feng, A. Xijun Hu, P.L. Yue, H.Y.Z. And, G.Q. Lu, Degradation of azo-dye Orange II by a photoassisted fenton reaction using a novel composite of iron oxide and silicate nanoparticles as a catalyst, Ind. Eng. Chem. Res., 42 (2003) 2058–2066.
[48] S.C. Elaoud, M. Panizza, G. Cerisola, T. Mhiri, Coumaric acid degradation by electro-Fenton process, J. Electroanal. Chem., 667 (2012) 19–23.
[49] M. Zhou, Q. Yu, L. Lei, G. Barton, Electro-Fenton method for the removal of methyl red in an efficient electrochemical system, Sep. Purif. Technol., 57 (2007) 380–387.
[50] W. He, X. Yan, H. Ma, J. Yu, J. Wang, X. Huang, Degradation of methyl orange by electro-Fenton-like process in the presence of chloride ion, Desal. Wat. Treat., 51 (2013) 6562–6571.

[51] D. Bao, X. Zhang, C. Guo, Z. Liu, L.I. Jing, Study on electro-catalytic oxidation of acid fuchsin using Ti/SnO_2,Ti/SnO_2-Sb_2O_3 anodes, Sichuan Building Sci., 37 (2011) 205–207.
[52] H.U. Feng-Ping, X.M. Wang, Z.M. Liu, Experimental study on electro-catalytic oxidation of acid fuchsin by PbO_2/Ti modified electrodes, Environ. Sci. Technol., 33 (2010) 51–54.
[53] F.C. Moreira, S. Garcia-Segura, V.J.P. Vilar, A.R.B. Rui, E. Brillas, Decolorization and mineralization of Sunset Yellow FCF azo dye by anodic oxidation, electro-Fenton, UVA photoelectro-Fenton and solar photoelectro-Fenton processes, Appl. Catal., B, 142–143 (2013) 877–890.
[54] E. Brillas, I. Sirés, M.A. Oturan, Electro-Fenton process and related electrochemical technologies based on Fenton's reaction chemistry, Chem. Rev., 109 (2009) 6570–6631.
[55] L. Labiadh, M.A. Oturan, M. Panizza, N.B. Hamadi, S. Ammar, Complete removal of AHPS synthetic dye from water using new electro-fenton oxidation catalyzed by natural pyrite as heterogeneous catalyst, J. Hazard. Mater., 297 (2015) 34–41.
[56] M. Sorour, M. Elsayed, N.A. El Moneem, H. Talaat, H. Shaalan, M.S. El, Free radical grafting kinetics of acrylamide onto a blend of starch/chitosan/alginate, Carbohydr. Polym., 98 (2013) 460–464.
[57] N. Sahiner, S. Butun, O. Ozay, B. Dibek, Utilization of smart hydrogel-metal composites as catalysis media, J. Colloid Interface Sci., 373 (2012) 122–128.
[58] S.A. Shahid, A.A. Qidwai, F. Anwar, I. Ullah, U. Rashid, Improvement in the water retention characteristics of sandy loam soil using a newly synthesized poly(acrylamide-co-acrylic acid)/$AlZnFe_2O_4$ superabsorbent hydrogel nanocomposite material, Molecules, 17 (2012) 9397–9412.
[59] O. Iglesias, M.A.F.D. Dios, M. Pazos, M.A. Sanromán, Using iron-loaded sepiolite obtained by adsorption as a catalyst in the electro-Fenton oxidation of Reactive Black 5, Environ. Sci. Pollut. Res., 20 (2013) 5983–5993.
[60] G.K. Parshetti, R.A. Doong, Dechlorination and photodegradation of trichloroethylene by Fe/TiO_2 nanocomposites in the presence of nickel ions under anoxic conditions, Appl. Catal., B, 100 (2010) 116–123.
[61] L. Jia, D.H.L. Ng, S. Peng, S. Yi, K. Chao, S. Liu, Synthesis of hierarchically porous Cu–Ni/C composite catalysts from tissue paper and their catalytic activity for the degradation of triphenylmethane dye in the microwave induced catalytic oxidation (MICO) process, Mater. Res. Bull., 64 (2015) 236–244.

Supplementary material

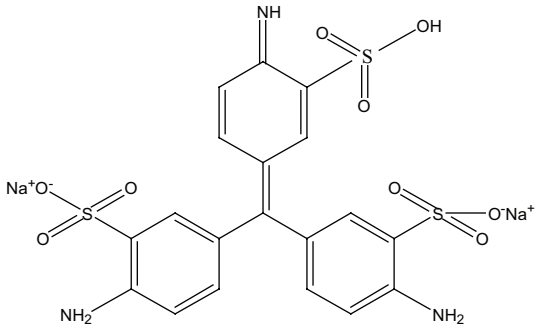

Molecular formula: $C_{20}H_{17}N_3Na_2O_9S_3$
CAS number: 3244-88-0

Fig. S1. Basic structure of AF.

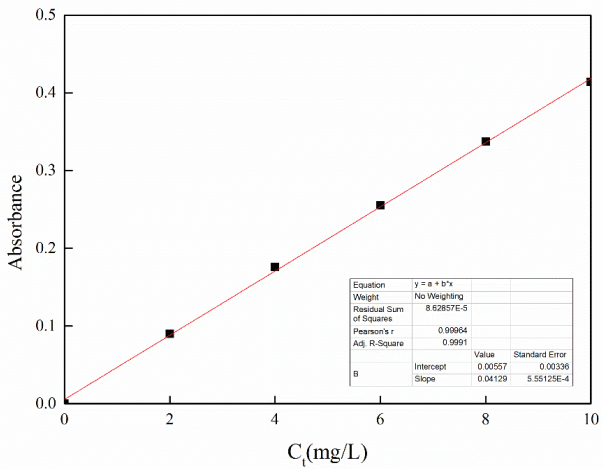

Fig. S2. Standard curve of AF.

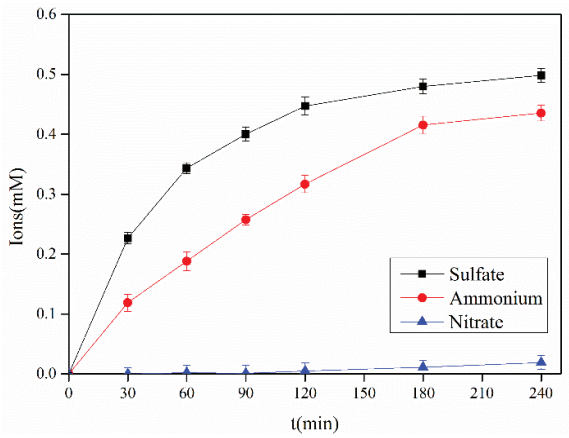

Fig. S3. Concentration evolution of inorganic ions formed during the electro-Fenton treatment of 100 mg/L AF in 0.05 mM Na_2SO_4 at pH 3 and 25°C with applied current of 300 mA in presence of H_2O_2/Fe^{3+}-SA ratio 0.4 as catalyst.

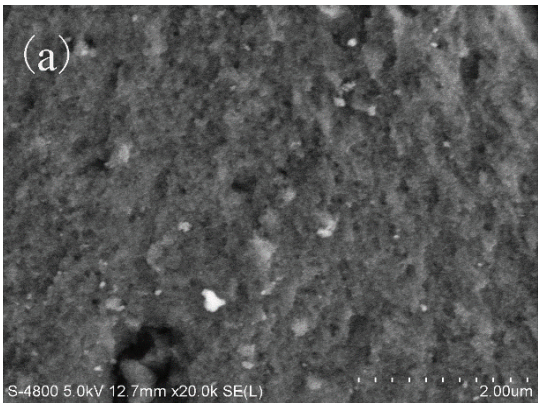

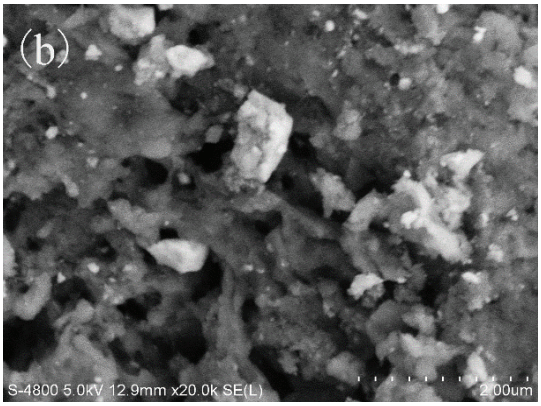

Fig. S4. SEM images of Fe^{3+}-SA (a) and Fe^{3+}-SA/EF (b).

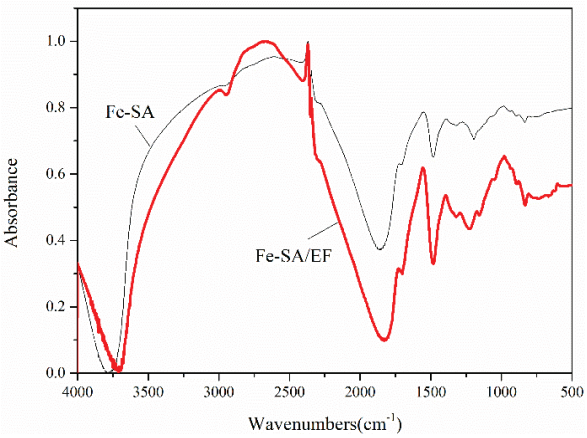

Fig. S5. FTIR spectra of Fe^{3+}-SA and Fe^{3+}-SA/EF.

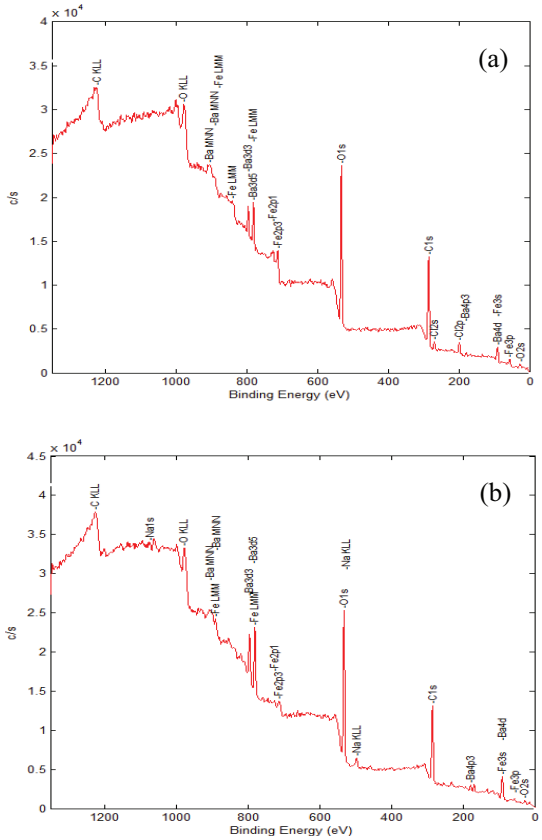

Fig. S6. XPS spectra of Fe^{3+}-SA (a) and Fe^{3+}-SA/EF (b).

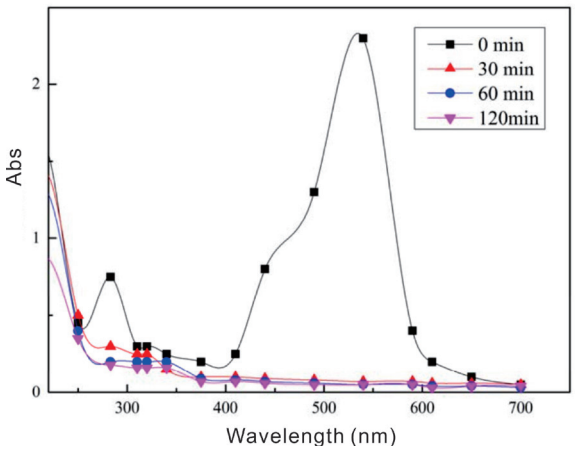

Fig. S7. UV–visible absorption spectrum of AF solution of different reaction time with 0.4 H_2O_2/Fe^{3+}-SA ratio, 0.05 M Na_2SO_4, 100 mg/L AF, 20 mA/cm^2 current density, and pH 3.

Table S1
Conditions for each test during EF

Influencing factor	pH	Current density	AF concentration	H_2O_2/Fe^{3+}-SA ratio	Concentration of Cl^-
pH	3	20	100	0.4	0
	5	20	100	0.4	0
	7	20	100	0.4	0
	9	20	100	0.4	0
	11	20	100	0.4	0
Current density	3	5	100	0.4	0
	3	10	100	0.4	0
	3	15	100	0.4	0
	3	20	100	0.4	0
	3	25	100	0.4	0
AF concentration	3	20	100	0.4	0
	3	20	200	0.4	0
	3	20	300	0.4	0
	3	20	400	0.4	0
H2O2/Fe^{3+}-SA ratio	3	20	200	0.1	0
	3	20	300	0.2	0
	3	20	400	0.4	0
	3	20	500	0.8	0
Concentration of Cl^-	3	20	100	0.4	0
	3	20	100	0.4	0.001
	3	20	100	0.4	0.01
	3	20	100	0.4	0.1

Table S2
Absorbance of different concentrations of standard AF

AF concentration	0	2	4	6	8	10
Absorbance	0.000	0.09	0.176	0.255	0.337	0.414

Table S3
Comparison of the maximum decolorization rate of AF by different treatment methods

Treatment method	Decolorization rate	Reference
Electro-catalytic oxidation by Fe-doped PbO_2/Ti electrodes	91.86%	[52]
Electro-catalytic oxidation by Ni-doped PbO_2/Ti electrodes	93.04%	[52]
Electro-catalytic oxidation by Ti/SnO_2-Sb_2O_3 electrodes	95.41%	[53]
Electro-catalytic oxidation by Ti/SnO_2 electrodes	50%	[53]
Electro-Fenton (EF) technique using Fe sodium alginate gel beads (Fe^{3+}-SA)	98.2%	This work

Table S4
Chemical composition of Fe^{3+}-SA and Fe^{3+}-SA/EF

Element	C1s	O1s	Na1s	Cl2p	Fe2p3	Ba3d5
Relative atomic ratio of Fe^{3+}-SA	58.37 ± 0.02	36.61 ± 0.02	0	2.15 ± 0.01	2.17 ± 0.01	0.69 ± 0.02
Relative atomic ratio of Fe^{3+}-SA/EF	60.72 ± 0.02	36.96 ± 0.02	0.61 ± 0.01	0	0.58 ± 0.01	1.13 ± 0.01

Table S5
Chemical composition of AF and AF/EF

	Ba (mg/L)	Fe (mg/L)
AF	0.015 ± 0.001	0.082 ± 0.001
AF/EF	0.016 ± 0.001	0.076 ± 0.001